Steel and Composite Structures, *Vol. 30, No. 6 (2019) 567-576*
DOI: https://doi.org/10.12989/scs.2019.30.6.567

Time-dependent creep analysis of a functionally graded beam with trapezoidal cross section using first-order shear deformation theory

Manouchehr Mohammad Hosseini Mirzaei [a], Abbas Loghman [*] and Mohammad Arefi [b]

Department of Solid Mechanics, Faculty of Mechanical Engineering, University of Kashan, I.R. Iran

(*Received March 1, 2018, Revised February 18, 2019, Accepted March 10, 2019*)

Abstract. Time-dependent creep analysis of a rotating functionally graded cantilever beam with trapezoidal longitudinal cross section subjected to thermal and inertia loading is investigated using first-order shear deformation theory (FSDT). The model described in this paper is a simple simulation of a turbine blade working under creep condition. The material is a metal based composite reinforced by a ceramic where the creep properties of which has been described by the Sherby's constitutive model. All mechanical and thermal properties except Poisson's ratio are assumed to be variable longitudinally based on the volume fraction of constituent. The principle of virtual work as well as first order shear deformation theory is used to derive governing equations. Longitudinal distribution of displacements and stresses are investigated for various volume fractions of reinforcement. Method of successive elastic solution is employed to obtain history of stresses and creep deformations. It is found that stresses and displacements approach their steady state values after 40000 hours. The results presented in this paper can be used for selection of appropriate longitudinal distribution of reinforcement to achieve the desired stresses and displacements.

Keywords: time-dependent creep; successive elastic solution; functionally graded trapezoidal beam; first-order shear deformation theory (FSDT)

1. Introduction

Normally turbine blades are working under high temperature and high stress levels due to combustion and high rotational speed. Creep is the most damaging mechanism exhausting the life of these components. Creep can cause gradual longitudinal deformation and elongation of the blade which must definitely be considered in the design of these elements. Although three dimensional creep deformations occur for the blade, but longitudinal displacement due to creep is much more important than the lateral deformations. Analytical creep solution cannot be obtained due to complex geometry of the blades and time-dependency of the problem. A simple cantilever rotating beam with trapezoidal longitudinal cross section and rectangular lateral cross section is considered in this paper to get an idea of general trend of longitudinal creep deformation under high temperature and centrifugal body force. A comprehensive literature survey on the time-dependent creep analysis is presented to justify necessity and novelties of the present work. The literature survey is also including application of various shear deformation theories to various structures.

Loghman and Wahab (1996) investigated creep stresses, strains and damages of thick-walled tubes subjected to an internal pressure and a thermal gradient by using the ɵ projection concept. They described a numerical model developed for the computation of creep damages in a thick-walled tube. Creep stress redistribution analysis of a thick-walled FGM cylinder subjected to uniform magnetic and temperature fields and under an internal pressure was investigated by Loghman *et al*. (2010). They found from history of stresses that radial stress redistributions are not considerable for different material properties, but significant changes occur for circumferential and effective stresses. History of strains, stresses, deformations and electric potentials of hollow cylinders made from PZT_5 have been investigated using Mendelson's method of successive elastic solution by Ghorbanpour Arani *et al*. (2011). Based on research of Loghman and Wahab (1996) and results of (Kordkheili and Naghdabadi 2007), Loghman *et al*. investigated time-dependent creep stress redistribution analysis of rotating disk, spheres and cylinder made of functionally graded composite (Loghman *et al*. 2011, 2017). Time-dependent electro magneto thermoelastic creep response of rotating disk made of functionally graded piezoelectric materials (FGPM) is studied by Loghman *et al*. (2013). It has been found that tensile radial stress distribution decreases during the life of the FGPM rotating disk which is associated with major electric potential redistributions which can be used as a sensor for condition monitoring of the FGPM rotating disk. Golmakaniyoon and Akhlaghi studied time-dependent thermoelastic creep behavior of functionally graded beams made of Al-SiC under in-plane thermal loading (Golmakaniyoon and Akhlaghi 2016). Steady state heat conduction from bottom

*Corresponding author, Professor,
E-mail: aloghman@kashanu.ac.ir
[a] Ph.D. Student
[b] Assistant Professor,
E-mail: arefi@kashanu.ac.ir; arefi63@gmail.com

ISSN: 1229-9367 (Print), 1598-6233 (Online)

to top surface was included in the problem.

Kapania and Raciti presented review about static, vibration and buckling analysis of beams and plates based on various shear deformation theories (Kapania and Raciti 1989). They also presented another work about delamination buckling in beams and plates. Shi et al. employed higher order shear deformation theory for finite element analysis of composite beams and plates (Shi *et al*. 1998). They found that the present composite beam element is more accurate than the higher-order beam elements. Kadoli *et al*. investigated static behavior of FG beams using higher order shear deformation theory (Kadoli *et al*. 2008). They showed distribution of transverse shear stress profile depends on the metal–ceramic combination. Nguyen *et al*. developed static and free vibration of axially loaded FG beams based on the first order shear deformation theory (Nguyen *et al*. 2013). They found that their model is efficient in analyzing static and free vibration problem of FG beams. Arefi *et al*. presented two-dimensional thermoelastic analysis of a functionally graded cylindrical pressure vessel subjected to axially variable thermal and mechanical loads using the first-order shear deformation theory (Arefi *et al*. 2016). The obtained results indicated that the boundary conditions of the cylinder have significant effect on thermoelastic response of the vessel. Arefi and Zenkour presented the governing equations of motion for a sandwich curved beam including an elastic core and two piezo-magnetic face-sheets using the first-order shear deformation theory (Arefi and Zenkour 2017a). They studied the influence of important parameters of the presented model on the electro-mechanical responses of the problem. In another article they derived the governing equations of bending analysis of a sandwich microbeam using higher-order sinusoidal shear deformation beam theory (Arefi and Zenkour 2017b). They showed that various types of parameters such as foundation, material and loads parameters have significant effect on the bending results.

Rao and Vyas studied the influence of nonlinear damping and transient conditions on the stress distribution of blades under constant speed (Rao and Vyas 1996). The beam model was used for analysis of the problem. Sankar obtained an elasticity solution for a functionally graded beam subjected to transverse loads (Sankar 2001). The gradation of material properties was accounted for Young's modulus along the thickness direction of beam. Base on this paper, Sankar and Tzeng investigated thermal stresses in FG beams (Sankar and Tzeng 2002). Chakrabortya *et al*. developed a new beam element for investigating the thermoelastic behavior of functionally graded beam structures (Chakraborty *et al*. 2003) based on first-order shear deformation theory. Li presented a new unified approach for analyzing the static and dynamic behaviors of functionally graded beams with the body force and shear deformation (Li 2008). A static result presented for a cantilever functionally graded beams and two wave speeds are obtained when using the Timoshenko beam theory. Arefi and Rahimi (2012) presented three-dimensional multi-field equations of a FGP thick shell with variable thickness, curvature and arbitrary nonhomogeneity based on curvilinear coordinate system.

Kiani and Eslami studied buckling analysis of beams made of functionally graded material under various types of thermal and boundary conditions (Kiani and Eslami 2010). Niknam et al. studied non-linear bending analysis of tapered functionally graded (FG) beam subjected to thermal and mechanical loads with general boundary condition (Niknam *et al*. 2014). In this article, in the case of no axial force along the beam a close form solution was presented but for the general case with axial force, the Galerkin technique was employed. Oh and Yoo presented a new method for vibration analysis of rotating pre-twisted tapered blades made of functionally graded materials (Oh and Yoo 2016). They investigated effects of the volume fraction index, Young's modulus ratio, hub radius ratio, pre-twist angle, taper ratios, width-to-thickness ratio and angular speed upon the dimensionless natural frequencies of the FG blade. Sahan (2015) presented an alternative analytical method for transient vibration analysis of doubly-curved laminated shells subjected to dynamic loads. Brnić *et al*. (2016) studied some mechanical, creep and fatigue properties of low alloy 42CrMo4 steel at different temperatures. Two dimensional time-dependent creep analysis of a thick-walled FG cylinder based on first order shear deformation theory was studied by Loghman *et al*. (2018).

The literature review on the creep analysis of various structures, functionally graded materials and various shear deformation theories was presented in Introduction section. One can conclude that although some important works about functionally graded materials were published, however no gradation of material properties along the longitudinal direction was mentioned. Due to this incompleteness and based on best author's knowledge, the creep analysis of trapezoidal beam made of functionally graded materials based on first order shear deformation theory can be observed in detail. In this paper, it is assumed that all material properties except Poisson ratio are graded along the longitudinal direction. After calculation of stresses, strains and displacements of blade due to thermal and mechanical loads, the history of them are evaluated based on creep analysis.

2. Creep behavior and material properties distribution

In this section the geometry and material properties of used model is presented. In addition, before presentation of full governing equations of the problem, the constitutive relations for creep behavior are introduced.

A variable thickness beam with a root thickness t_r and tip thickness t_t is considered. Variable mechanical and thermal loads are applied on the beam. Boundary condition at the root of beam is assumed fixed and tip of beam is assumed free. The beam is rotating with a constant angular velocity $\omega = 7800\ rpm$. The longitudinal variable pressure is assumed linear as: $P(x) = -10^{-2}\left(2 + 3\,{}^{x}/_{L}\right)\ MPa$ due to aerodynamic forces act on the top surface of the beam. 567-The other parameters of the problem are assumed as: $T_r = 500^o K, T_t = 600^o K. r_0 = 300\ mm.$

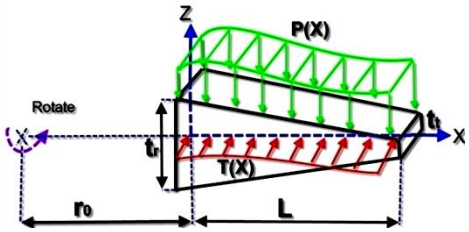

Fig. 1 Geometry and loading conditions for the rotating FGM beam

The geometry and loading conditions are shown in Fig. 1.

The distribution of reinforcement particles is assumed to be linear from root to tip of the beam as follows

$$VF(x) = VF_{root} + \frac{x}{L} \times (VF_{tip} - VF_{root}) \tag{1}$$

where VF_{root} and VF_{tip} are volume fractions of reinforcement at root and tip of the beam, respectively. In this article, all mechanical and thermal properties except Poisson's ratio are supposed to be longitudinal variable based on volume percent of reinforcement content by

$$PR(x) = PR_{matrix} + \left(PR_{reinforcement} - PR_{matrix}\right) \times \frac{VF(x)}{100} \tag{2}$$

where PR(x) is an arbitrary longitudinally variable material property. PR_{matrix} is matrix property, $PR_{reinforcement}$ is pure reinforcement property, and VF(x) is volume fraction of reinforcement at x.

According to Eq. (2), longitudinal-dependent properties such as elasticity modulus, shear modulus, density and coefficients of heat expansion are written as follows

$$\begin{aligned} E(x) &= E_{matrix} + (E_{reinforcement} - E_{matrix}) \times \frac{VF(x)}{100} \\ G(x) &= G_{matrix} + (G_{reinforcement} - G_{matrix}) \times \frac{VF(x)}{100} \\ \alpha(x) &= \alpha_{matrix} + (\alpha_{reinforcement} - \alpha_{matrix}) \times \frac{VF(x)}{100} \\ \rho(x) &= \rho_{matrix} + (\rho_{reinforcement} - \rho_{matrix}) \times \frac{VF(x)}{100} \end{aligned} \tag{3}$$

The following data for matrix and reinforcement properties are used in this investigation (Gupta *et al*. 2004)

$$\begin{aligned} E_{Al} &= 70Gpa & E_{sic} &= 410Gpa \\ G_{Al} &= 27Gpa & G_{sic} &= 41.5Gpa \\ \alpha_{Al} &= 23.1 \times 10^{-6}K^{-1} & \alpha_{sic} &= 4 \times 10^{-6}K^{-1} \\ \rho_{Al} &= 2700kgm^{-3} & \rho_{sic} &= 3200kgm^{-3} \end{aligned} \tag{4}$$

Fig. 2 shows three longitudinal distributions of reinforcement that are used in this study. These are (a) pure matrix; (b) matrix with 30% reinforcement at root of beam and pure matrix at tip of beam; (c) pure matrix at the root of beam and 30% reinforcement at the tip of beam.

Fig. 2 Longitudinal cross section of beam different composition cases of a, b and c

After completion of geometrical explanations of the problem and distribution of reinforcement along the longitudinal direction, it is necessary to describe the constitutive relations for creep behavior of materials. To model the creep behavior of reinforced polymer composite, Sherby's constitutive model is used as follows

$$\dot{\varepsilon_c} = [M(\sigma_e - \sigma_0)]^n \tag{5}$$

where $\dot{\varepsilon_c}$ is effective creep strain rate and σ_e is the effective stress. The value of n is taken to be 8 and the creep parameters M and σ_0 are taken from (Gupta *et al*. 2004).

$$\begin{aligned} \ln \mathrm{M} &= 0.2077 \ln \mathrm{D(x)} - 35.38 \\ &\quad -0.622 \ln VF(\mathrm{x}) + 4.98 \ln \mathrm{T(x)} \\ \sigma_0 &= 0.01057\, T(x) + -0.03507\mathrm{D(x)} \\ &\quad -2.11916 + 1.00536\, VF(x) \end{aligned} \tag{6}$$

In this article, particle size is assumed constant (D(x) = 1.7 μm). D(x) is the particle size in μm, T(x) is the temperature distribution and VF(x) is volume fraction of SiC particle at point of x.

3. Time dependent creep formulation

3.1 Thermo-elastic analysis based on FSDT

In this section, FSDT is implemented to describe the displacement field of the beam in terms of deformation of mid-surface and rotation about outward axis of the mid-surface (Mirsky 1959). By using this theory, the longitudinal and transverse deformation components are expressed by combination of displacement and rotation components as follows

$$\begin{aligned} \mathrm{u(x,z)} &= \mathrm{u_0(x)} + \mathrm{z}\psi\mathrm{(x)} \\ \mathrm{w(x,z)} &= \mathrm{w_0(x)} \end{aligned} \tag{7}$$

where $\mathrm{u(x,z)}$, $\mathrm{w(x,z)}$ are the longitudinal and transverse components of displacement, respectively. $\mathrm{u_0}$, $\mathrm{w_0}$ are longitudinal and transverse deformation of middle surface and $\psi(\mathrm{x})$ is rotation component. With regard to kinematic relation (7), the strain components is written as

$$\begin{aligned} \varepsilon_{xx} &= \frac{\partial u}{\partial x} = \frac{\partial u_0}{\partial x} + z\frac{\partial \psi(x)}{\partial x} + \alpha T(x) \\ \gamma_{xz} &= \frac{\partial u}{\partial z} + \frac{\partial w}{\partial x} = \psi(x) + \frac{\partial w_0}{\partial x} \end{aligned} \tag{8}$$

Stress components in terms of strain components and temperature distribution are presented as follows

$$\sigma_{xx} = E\left[\frac{\partial u_0}{\partial x} + z\frac{\partial \psi(x)}{\partial x} + \alpha T(x)\right]$$
$$\tau_{xz} = G\left[\psi(x) + \frac{\partial w_0}{\partial x}\right] \quad (9)$$

The principle of virtual work is used to derive governing equations as follows

$$\delta U = \int_A \int_z (\tau_{xz}\delta\gamma_{xz} + \sigma_{xx}\delta\varepsilon_{xx})dzdA$$
$$= \int_A (N_{xz}\delta\psi + N_{xz}\frac{\partial\delta w_0}{\partial x} + N_{xx}\frac{\partial\delta u_0}{\partial x} + M_{xx}\frac{\partial\delta\psi}{\partial x})dx \quad (10)$$

In which the resultant components are expressed as

$$N_{xx} = \int_{-\frac{g(x)}{2}}^{\frac{g(x)}{2}} \sigma_{xx}dz = \left[\int_{-\frac{g(x)}{2}}^{\frac{g(x)}{2}} E(x)dz\right]\frac{\partial u_0}{\partial x} + \left[\int_{-\frac{g(x)}{2}}^{\frac{g(x)}{2}} zE(x)dz\right]\frac{\partial\psi}{\partial x} + \int_{-\frac{g(x)}{2}}^{\frac{g(x)}{2}} E(x)\alpha(x)T(x)dz$$
$$N_{xz} = \int_{-\frac{g(x)}{2}}^{\frac{g(x)}{2}} \sigma_{xz}dz = \left[\int_{-\frac{g(x)}{2}}^{\frac{g(x)}{2}} G(x)dz\right]\left[\psi(x) + \frac{\partial w_0}{\partial x}\right] \quad (11)$$
$$M_{xx} = \int_{-\frac{g(x)}{2}}^{\frac{g(x)}{2}} z\sigma_{xx}dz = \left[\int_{-\frac{g(x)}{2}}^{\frac{g(x)}{2}} zE(x)dz\right]\frac{\partial u_0}{\partial x} + \left[\int_{-\frac{g(x)}{2}}^{\frac{g(x)}{2}} z^2E(x)dz\right]\frac{\partial\psi}{\partial x} + \int_{-\frac{g(x)}{2}}^{\frac{g(x)}{2}} E(x)\alpha(x)T(x)zdz$$

where $g(x) = t_r - (t_r - t_t)x/L$.

The external work due to body force and external force is derived as Eq. (13)

$$W = -\int_x [L_1(x)u + L_2(x)\psi + L_3(x)w]\,dx \quad (12)$$

In which the vector of applied force is introduced as

$$L(x) = \begin{bmatrix} L_1(x) \\ L_2(x) \\ L_3(x) \end{bmatrix} = \begin{bmatrix} \omega^2\rho(x)h(x)[r_0 + x] \\ 0 \\ -P(x) \end{bmatrix} \quad (13)$$

and variation of external work can be written as

$$\delta W = -\int_z L_1(x)\delta u + L_2(x)\delta\psi + L_3(x)\delta w\,dx \quad (14)$$

After applying the integration by part and arranging the variables, the governing equations can be derived as

$$\delta u_0:\ B_5(x)T(x) + \frac{\partial N_{xx}}{\partial x} = L_1(x)$$
$$\delta\psi:\ N_{xz} - \frac{\partial M_{xx}}{\partial x} = 0 \quad (15)$$
$$\delta w:\ B_6(x)T(x) + \frac{\partial N_{xz}}{\partial x} = L_3(x)$$

Substituting Eq. (11) into Eq. (15) the following differential equation is obtained

$$B_1(x)u_{,xx} + B_2(x)\psi_{,xx} + B_5(x)T(x) = L_1(x)$$
$$-B_2(x)u_{,xx}(x) - B_4(x)\psi_{,xx}(x)$$
$$+B_3(x)\psi(x) + B_3(x)w_{,x}(x) = 0 \quad (16)$$
$$B_3(x)\psi_{,x}(x) + B_3(x)w_{,xx}(x) + B_6(x)T(x) = L_3(x)$$

In Eqs. (15) and (16), B_i (i = 1 . . . 6) are presented in Appendix A.

To solve these second-order ordinary differential equations with variable coefficients, semi-analytical approach known as the division method is employed (Kordkheili and Naghdabadi 2007). Based on this method, the solution domain is divided into a finite number of sub-domains (Fig. 3).

With regard to second and tertiary relation of Eq. (15) can be written as

$$-\frac{\partial M_{xx}}{\partial x} + N_{xz} = 0 \rightarrow \frac{\partial^2 M_{xx}}{\partial x^2} = \frac{\partial N_{xz}}{\partial x} \rightarrow \frac{\partial^2 M_{xx}}{\partial x^2} = L_3(x^k) - B_6(x^k)T(x^k) \quad (17)$$

In which k = 1, 2, 3,…, m.

Eqs. (15) and (16) are substituted into Eq. (17) for every section.

$$\frac{\partial M_{xx}}{\partial x} = B_2(x^k)u_{,xx}(x^k) + B_4(x^k)\psi_{,xx}(x^k)$$
$$= \frac{B_2(x^k)}{B_1(x^k)}\begin{pmatrix} -B_2(x^k)\psi_{,xx}(x^k) \\ +L_1(x^k) - B_5(x)T(x) \end{pmatrix}$$
$$+B_4(x^k)\psi_{,xx}(x^k) \quad (18)$$
$$= \left(B_4(x^k) - \frac{(B_2(x^k))^2}{B_1(x^k)}\right)\psi_{,xx}(x^k)$$
$$+\frac{B_2(x^k)}{B_1(x^k)}(L_1(x^k) - B_5(x)T(x))$$

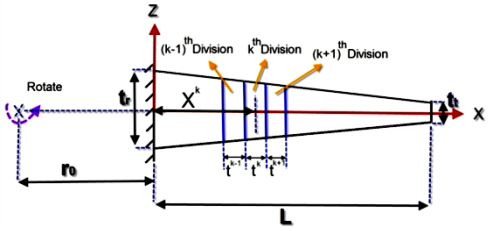

Fig. 3 Division of the beam into a finite number of subdomains

For using of second section of Eq. (17), we compute differential from Eq. (18) and then first relation of Eq. (16) is substituted into Eq. (17) as follows

$$\begin{aligned}\frac{\partial^2 M_{xx}}{\partial x^2} &= \left(B_4(x^k) - \frac{(B_2(x^k))^2}{B_1(x^k)}\right)\psi_{,xxx}(x^k) \\ &+ \frac{B_2(x^k)}{B_1(x^k)}(L_{1,x}(x^k) - B_5(x)T_{1,x}(x) \\ &= L_3(x^k) - B_6(x)T(x)\end{aligned} \tag{19}$$

$\psi_{,xxx}(x^k)$, $u_{,xx}(x^k)$ and $w_{,x}(x^k)$ are calculated at all division points as follows

$$\begin{aligned}&\psi_{,xxx}(x^k) \\ &= \frac{B_1(x^k)\big(L_3(x^k) - B_6(x)T(x)\big) - B_2(x^k)(L_{1,x}(x^k) - B_5(x)T_{,x}(x))}{B_1(x^k)B_4(x^k) - (B_2(x^k))^2}u_{,xx}(x^k) \\ &= \frac{1}{B_1(x^k)}\big(L_1(x^k) - B_2(x^k)\psi_{,xx}(x^k) - B_5(x)T(x)\big)\end{aligned} \tag{20}$$

$$\begin{aligned}&w_{,x}(x^k) \\ &= \frac{1}{B_3(x^k)}\begin{pmatrix}B_2(x^k)u_{,xx}(x^k) + B_4(x^k)\psi_{,xx}(x^k) \\ -B_3(x^k)\psi(x^k)\end{pmatrix}\end{aligned}$$

The continuity relations between two adjacent divisions are expressed as

$$\begin{aligned}u\left(x^k + \frac{t^k}{2}\right) &= u\left(x^{k+1} - \frac{t^{k+1}}{2}\right) \\ \psi\left(x^k + \frac{t^k}{2}\right) &= \psi\left(x^{k+1} - \frac{t^{k+1}}{2}\right) \\ w\left(x^k + \frac{t^k}{2}\right) &= w\left(x^{k+1} - \frac{t^{k+1}}{2}\right) \\ \frac{du}{dx}\left(x^k + \frac{t^k}{2}\right) &= \frac{du}{dx}\left(x^{k+1} - \frac{t^{k+1}}{2}\right) \\ \frac{d\psi}{dx}\left(x^k + \frac{t^k}{2}\right) &= \frac{d\psi}{dx}\left(x^{k+1} - \frac{t^{k+1}}{2}\right) \\ \frac{dw}{dx}\left(x^k + \frac{t^k}{2}\right) &= \frac{dw}{dx}\left(x^{k+1} - \frac{t^{k+1}}{2}\right)\end{aligned} \tag{21}$$

The boundary conditions of the problem are presented for root and tip of the beam as follows

$$\text{B. c:}\begin{cases}u = 0 \\ \psi = 0 \\ w = 0\end{cases} \qquad x = 0$$

$$\text{B. c:}\begin{cases}N_{xz} = \int \tau(x,z)dA = 0 \\ M_{xx} = \int z\sigma_{xx}\,dA = 0 \\ N_{xx} = \int \sigma_{xx}\,dA = 0\end{cases} \qquad x = L \tag{22}$$

The updated integration constants are presented in Appendix B.

By increasing the number of sub-domains, the accuracy of numerical results can be improved.

3.1 Time-dependent creep analysis

For time-dependent creep analysis, creep strains are included into the stress-strain relations. Total stresses are the sum of elastic, thermal, and creep stresses as follows

$$\begin{aligned}\sigma_{xx} &= \frac{E}{(1+\nu)(1-2\nu)}[(1-\nu)\varepsilon_{xx} + \nu(\varepsilon_{xx} + \varepsilon_{xx})] \\ &- \frac{E}{1-2\nu}\alpha T \\ &- \frac{E}{(1+\nu)(1-2\nu)}[(\varepsilon^c_{xx} + \nu(\varepsilon^c_{yy} + \varepsilon^c_{zz})] \\ \tau_{xz} &= \tau_{xz}^{elastic} - 2G\varepsilon^c_{xz}\end{aligned} \tag{23}$$

where ε^c_{xx}, ε^c_{yy} and ε^c_{zz} are creep strains along x, y and z directions respectively and ε^c_{xz} is creep strain in x-z plane. Creep strains are depending on time, temperature and stress. According to the Prandtl–Reuss relations, creep strain increments are related to the current stresses and the material uni-axial creep behavior (Mendelson 1968) as follows

$$\begin{aligned}\Delta\varepsilon^c_{xx} &= \frac{\Delta\varepsilon^c_e}{2\sigma_e}(2\sigma_{xx}) \\ \Delta\varepsilon^c_{zz} &= \frac{\Delta\varepsilon^c_e}{2\sigma_e}(-\sigma_{xx}) \\ \Delta\varepsilon^c_{yy} &= -\Delta\varepsilon^c_{xx} - \Delta\varepsilon^c_{zz} \\ \Delta\varepsilon^c_{xz} &= \frac{3\Delta\varepsilon^c_e}{2\sigma_e}(\tau_{xz})\end{aligned} \tag{24}$$

where $\Delta\varepsilon^c_{xx}$, $\Delta\varepsilon^c_{yy}$ and $\Delta\varepsilon^c_{zz}$ are increment of creep normal strain along x, y, z directions respectively and $\Delta\varepsilon^c_{xz}$ is increment of shear strain. Also, $\Delta\varepsilon^c_e$ and σ_e are equivalent creep strain increment and equivalent stress, respectively. Third relation of Eq. (24) is obtained from the incompressibility condition. Equivalent and effective strain and stress are defined as follows

$$\begin{aligned}\Delta\varepsilon^c_e &= \frac{\sqrt{2}}{3}\sqrt{\frac{7}{2}(\Delta\varepsilon^c_{xx})^2 + 6(\Delta\varepsilon^c_{xz})^2} \\ \sigma_e &= \sqrt{{\sigma_{xx}}^2 + 3{\tau_{xz}}^2}\end{aligned} \tag{25}$$

By using the creep behavior model (Eq. (5)), the increment of creep strain is calculated in terms of time and effective stress as follows

$$\Delta\varepsilon_c = [M(\sigma_e - \sigma_0)]^n \Delta t \tag{26}$$

The history of stresses, strains and displacements can be calculated using Eqs. (23)-(26) based on method of successive elastic solution. The procedure of successive elastic solution is including seven steps that are presented as:

(1) An identical time interval is selected 3000s for timing steps of i'th step ($\Delta t_i = 3000s$). The total time is the sum of time intervals as

$$t_i = \sum_{j=1}^{i-1} \Delta t_j + \Delta t_i \tag{27}$$

(2) To start the creep analysis, an initial increment of strains must be assumed. The initial estimates of $\Delta\varepsilon^c_{xx.ik} = +0.0001$ and $\Delta\varepsilon^c_{xz} = -0.000102$ are selected for all sub-domains points (k) for i'th timing step.
Creep strain at any point throughout the length of the beam is the cumulative sum of all previous creep strains.

$$\begin{aligned}
\varepsilon^c_{xx,ik} &= \sum_{j=1}^{i-1} \Delta\varepsilon^c_{xx,jk} + \Delta\varepsilon^c_{xx,ik} \\
\varepsilon^c_{zz,ik} &= \sum_{j=1}^{i-1} \Delta\varepsilon^c_{zz,jk} + \Delta\varepsilon^c_{zz,ik} \\
\varepsilon^c_{xz,ik} &= \sum_{j=1}^{i-1} \Delta\varepsilon^c_{xz,jk} + \Delta\varepsilon^c_{xz,ik} \\
\Delta\varepsilon^c_{yy,ik} &= -(\Delta\varepsilon^c_{xx,ik} + \Delta\varepsilon^c_{zz,ik})
\end{aligned} \tag{28}$$

where the subscripts i and j imply the timing step and division point, respectively.

(3) With the initial estimates of creep strains increment and using Eq. (28), new axial and shear stresses can be calculated based on Eq. (23). Using the computed stresses, the initial estimates of strains and displacements and then current axial and shear stresses are computed.

(4) For all division points, effective stresses are calculated as follows

$$\sigma_{e,ik} = \sqrt{{\sigma_{xx,ik}}^2 + 3{\tau_{xz,ik}}^2} \tag{29}$$

(5) Then, effective creep strain are calculated at all division points (k) for the i'th timing step using the Sherby's creep constitutive model as follows

$$\Delta\varepsilon_{c,ik} = [M_k(\sigma_{e,ik} - \sigma_{0,k})]^8 \Delta t_i \tag{30}$$

where

$$\begin{aligned}
ln\, M_k &= 0.2077\, ln\, D_k(x) \\
&\quad +4.98\, ln\, T(x^k) - 0.622\, ln\, VF(x^k) - 35.38 \\
\sigma_{0,k} &= 0.01057\, T(x^k) + 1.00536\, VF(x^k) \\
&\quad -2.11916 - 0.03507 D_k(x)
\end{aligned} \tag{31}$$

In this article, value of particle size is assumed constant of $D_k(x) = 1.7\mu m$.

(6) From Prandtl–Reuss relations, new values of creep strain increments are obtained as follows

$$\begin{aligned}
\Delta\varepsilon^{c,new}_{xx,ik} &= \frac{\Delta\varepsilon^c_{e,ik}}{2\sigma_{e,ik}}(2\sigma_{xx,ik}) \\
\Delta\varepsilon^{c,new}_{zz,ik} &= \frac{\Delta\varepsilon^c_{e,ik}}{2\sigma_{e,k}}(-\sigma_{xx,ik}) \\
\Delta\varepsilon^{c,new}_{yy,ik} &= -\Delta\varepsilon^{c,new}_{xx.ik} - \Delta\varepsilon^{c,new}_{zz,ik} \\
\Delta\varepsilon^{c,new}_{xz,ik} &= \frac{3\Delta\varepsilon^c_{e,ik}}{2\sigma_{e,ik}}(\tau_{xz,ik})
\end{aligned} \tag{32}$$

(7) These new calculated values of creep strain increments are compared with the previous values for inspection of required convergence. If convergence is satisfied, time is advanced one increment and the procedure is repeated for the new time increment from step 1. If convergence is not obtained, these new calculated values of creep strain increments will be replaced as initial values and the procedure will be repeated from step 2.

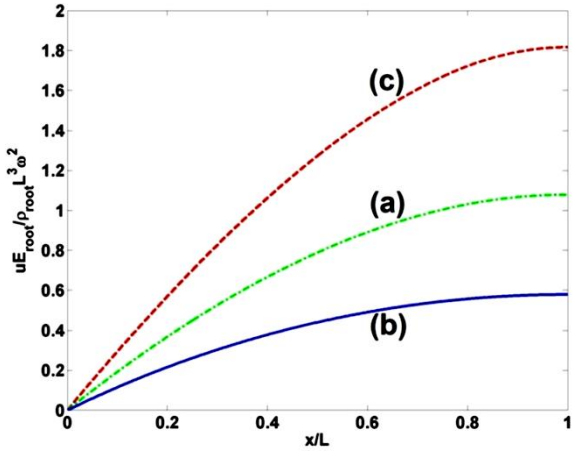

Fig. 4 Longitudinal distribution of dimensionless axial displacement of composite beam for various reinforcements

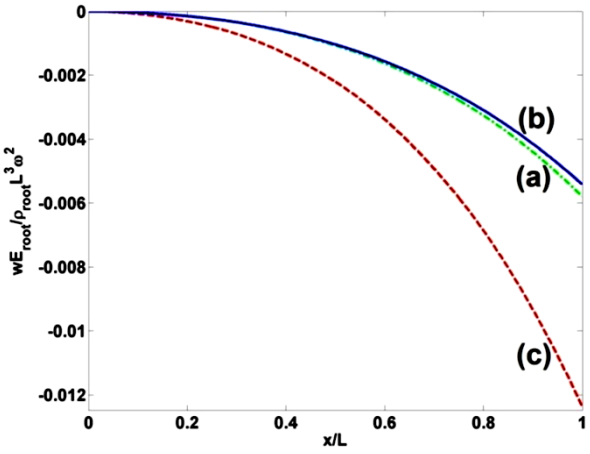

Fig. 5 Longitudinal distribution of dimensionless transverse displacement of composite beam for various reinforcements

4. Numerical results and discussion

In this section, the numerical results and corresponding conclusions are presented. This section is including the elastic results and history of them after various creep times.

4.1 Elastic results

Fig. 4 shows variation of dimensionless axial deformation of composite beam along the longitudinal direction for various distributions of reinforcement. The longitudinal distribution of transverse deformation of composite beam for various distributions of reinforcement is presented in Fig. 5. One can conclude that the higher deformations are achieved for pattern (c) and lower one for pattern (b).

Shown in Figs. 6, 7 and 8 are longitudinal variations of dimensionless axial, shear and effective stresses in terms of various distributions of reinforcement. It is observed that maximum normal, shear and effective stresses are presented for patterns c, a and a respectively. In addition the minimum normal, shear and effective stresses are presented for pattern b.

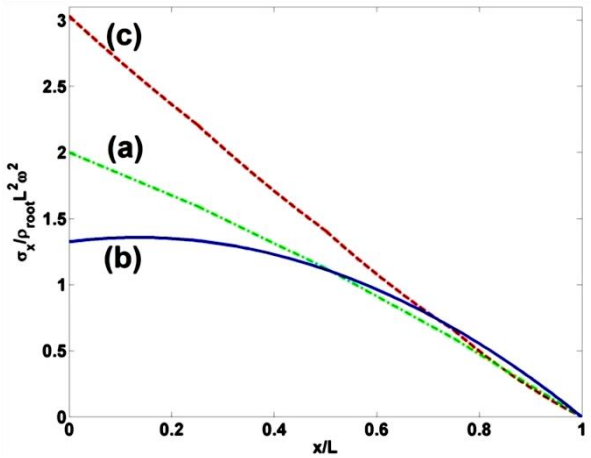

Fig. 6 Longitudinal distribution of dimensionless axial stress of composite beam for various reinforcements

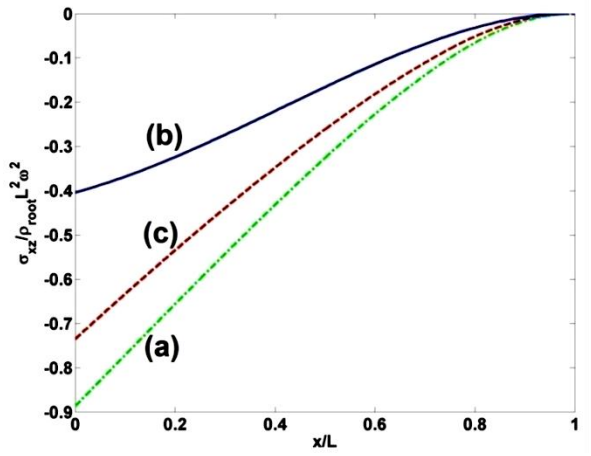

Fig. 7 Longitudinal distribution of dimensionless shear stress of composite beam for various reinforcements

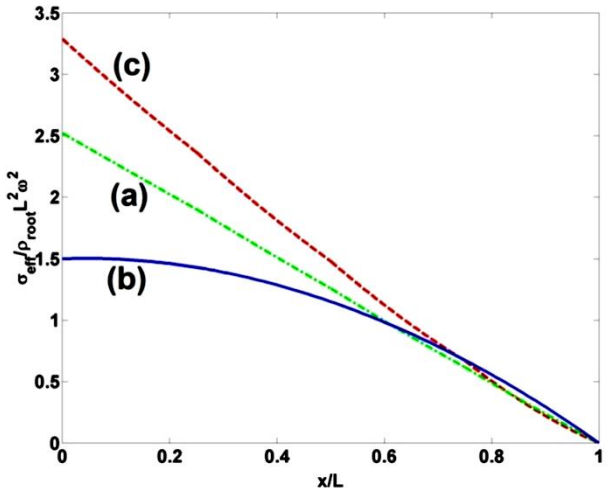

Fig. 8 Longitudinal distribution of dimensionless effective stress of composite beam for various reinforcements

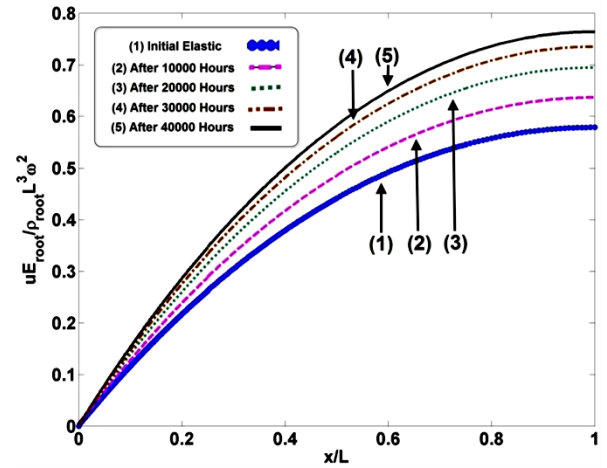

Fig. 9 History of dimensionless axial displacement of composite beam for various creep times and case b

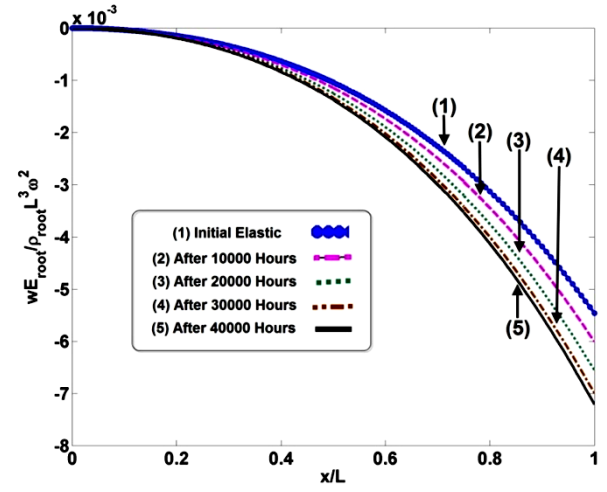

Fig. 10 History of dimensionless transverse displacement of composite beam for various creep times and case b

In continuation of the presentation of numerical results, the history of deformations, strains and stresses are provided.

Figs. 9 and 10 show longitudinal distributions of axial and transverse deformations of middle surface for various creep times (0, 10000, 20000, 30000 and 40000 hours). The numerical results indicate that with increase of creep time, the deformations are increased. In addition, it is observed that the rates of change of deformations are decreased for higher times and it reaches to an asymptotic value.

Figs. 11, 12 and 13 show longitudinal distributions of axial, shear and effective stresses for various creep times (0, 10000, 20000, 30000 and 40000 hours). The numerical results indicate that with increase of creep time, all stress components are decreased.

One can conclude that the rates of change of deformations are decreased for higher creep times and reaches to an asymptotic value.

Figs. 14, 15 show variation of creep normal and shear strains along the longitudinal direction for various creep

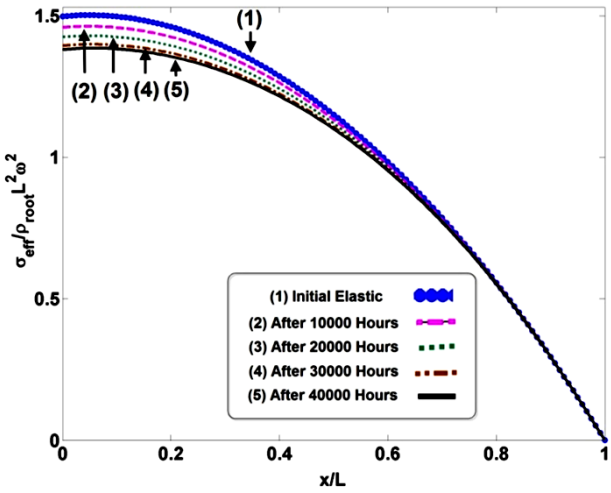

Fig. 13 History of dimensionless effective stress of composite beam for various creep times and case b

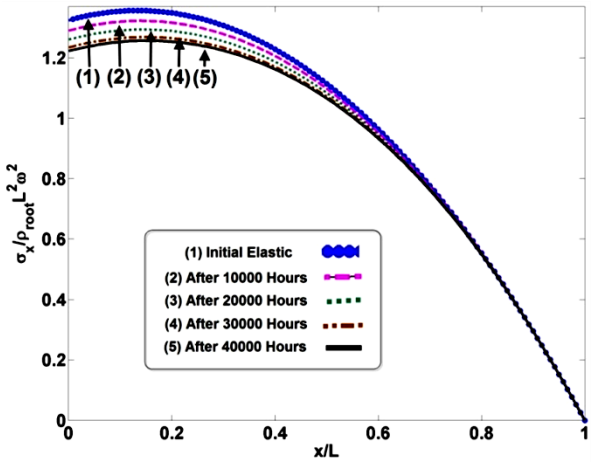

Fig. 11 History of dimensionless axial stress of composite beam for various creep times and case b

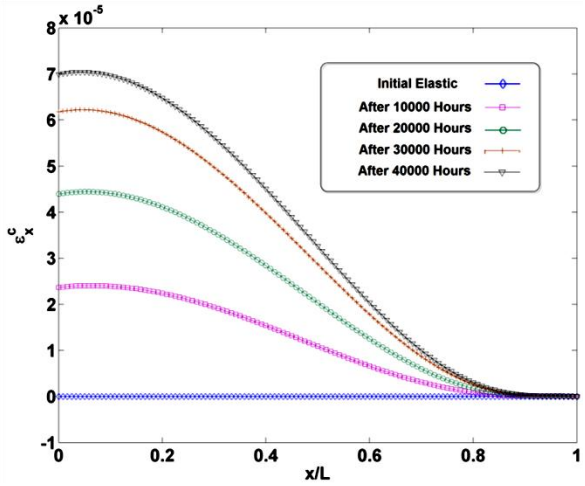

Fig. 14 History of creep normal strain of composite beam for various creep times and case b

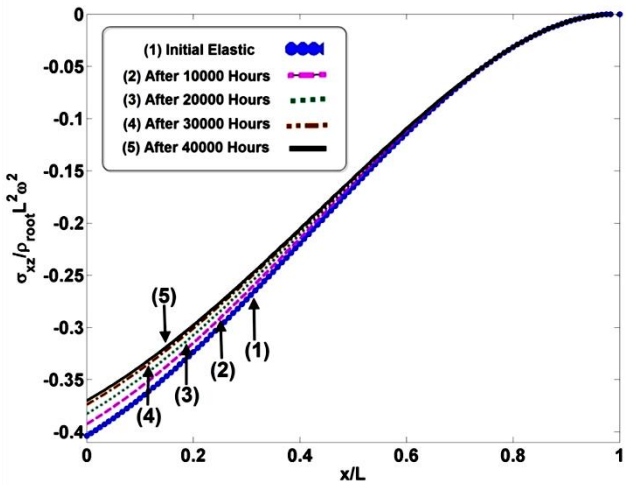

Fig. 12 History of dimensionless shear stress of composite beam for various creep times and case b

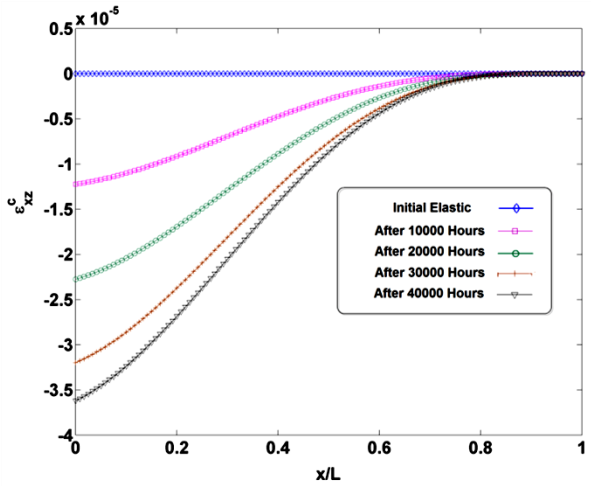

Fig. 15 History of creep shear strain of composite beam for various creep times and case b

times. It is concluded that with increase of creep times, the strains are increased significantly. The convergence condition can be observed for high creep times.

5. Conclusions

Time dependent creep analysis of a functionally graded beam with trapezoidal longitudinal cross section was studied in this paper. First order shear deformation theory was used for derivation of governing equations of a functionally graded beam subjected to longitudinally variable thermal and mechanical loads. The creep properties of structure were described by the Sherby's constitutive model. All mechanical and thermal properties except Poisson's ratio were assumed to be variable longitudinally based on the volume fraction of constituent. Method of successive elastic solution was employed to obtain history of stresses and creep deformations.

The numerical results were presented in terms of various important parameters along the longitudinal direction. Based on numerical results, it is concluded that minimum axial deflection distribution and maximum uniform distribution of axial, shear and effective thermoelastic stresses is illustrated in FGM beam of aluminum with a linear distribution of 0% SiC particles at root of the beam and 30% SiC particles at tip of the beam. In addition, the minimum axial deformation of functionally grade beam is reached for composite case b.

References

Arefi, M. and Rahimi, G.H. (2012), "Three-dimensional multi-field equations of a functionally graded piezoelectric thick shell with variable thickness, curvature and arbitrary nonhomogeneity", *Acta. Mech.*, **223**(1), 63-79.

Arefi, M. and Zenkour, A. (2017a), "Electro-magneto-elastic analysis of a three-layer curved beam", *Smart. Struct. Syst.*, *Int. J.*, **19**(6), 695-703.

Arefi, M. and Zenkour, A.M. (2017b), "Size-dependent electro-elastic analysis of a sandwich microbeam based on higher-order sinusoidal shear deformation theory and strain gradient theory", *J. Intel. Mater. Syst. Struct.*, **29**(7), 1394-1406.

Arefi, M., Faegh, R.K. and Loghman, A. (2016), "The effect of axially variable thermal and mechanical loads on the 2D thermoelastic response of FG cylindrical shell", *J. Therm. Stresses.*, **39**(12), 1539-1559.

Brnić, J., Čanađija, M., Turkalj, G., Kršćanski, S., Lanc, D., Brčić, M. and Zeng, G. (2016), "Short-time creep, fatigue and mechanical properties of 42CrMo4-low alloy structural steel", *Steel Compos. Struct., Int. J.*, **22**(4), 875-888.

Chakraborty, A., Gopalakrishnan, S. and Reddy, J.N. (2003), "A new beam finite element for the analysis of functionally graded materials", *Int. J. Mech. Sci.*, **45**(3), 519-539.

Ghorbanpour Arani, A., Mosallaie Barzoki, A.A., Kolahchi, R., Mozdianfard, M.R. and Loghman, A. (2011), "Semi-analytical solution of time-dependent electro-thermo-mechanical creep for radially polarized piezoelectric cylinder", *Comput. Struct.*, **89**(15), 1494-1502.

Golmakaniyoon, S. and Akhlaghi, F. (2016), "Time-dependent creep behavior of Al–SiC functionally graded beams under in-plane thermal loading", *Comput. Mater. Sci.*, **121C**, 182-190.

Gupta, V.K., Singh, S.B., Chandrawat, H.N. and Ray, S. (2004), "Steady state creep and material parameters in a rotating disc of Al–SiCP composite", *Eur. J. Mech-A/Solids*, **23**(2), 335-344.

Kadoli, R., Akhtar, K. and Ganesan, N. (2008), "Static analysis of functionally graded beams using higher order shear deformation theory", *Appl. Math. Model.*, **32**(12), 2509-2525.

Kapania, R.K. and Raciti, S. (1989), "Recent advances in analysis of laminated beams and plates. Part I - Shearеffects and buckling", *AIAA Journal*, **27**(7), 923-935.

Kiani, Y. and Eslami, M.R. (2010), "Thermal buckling analysis of functionally graded material beams", *Int. J. Mech. Mater. Des.*, **6**(3), 229-238.

Kordkheili, S.A.H. and Naghdabadi, R. (2007), "Thermoelastic analysis of a functionally graded rotating disk", *Compos. Struct.*, **79**(4), 508-516.

Li, X.F. (2008), "A unified approach for analyzing static and dynamic behaviors of functionally graded Timoshenko and Euler–Bernoulli beams", *J. Sound. Vib.*, **318**(4), 1210-1229.

Loghman, A. and Wahab, M.A. (1996), "Creep damage simulation of thick-walled tubes using the Θ projection concept", *Int. J. Pres. Ves. Pip.*, **67**(1), 105-111.

Loghman, A., Ghorbanpour Arani, A., Amir, S. and Vajedi, A. (2010), "Magnetothermoelastic creep analysis of functionally graded cylinders", *Int. J. Pres. Ves. Pip.*, **87**(7), 389-395.

Loghman, A., Ghorbanpour Arani, A., Shajari, A.R. and Amir, S. (2011), "Time-dependent thermoelastic creep analysis of rotating disk made of Al–SiC composite", *Arch. Appl. Mech.*, **81**(12), 1853-1864.

Loghman, A., Abdollahian, M., Jafarzadeh Jazi, A. and Arani, A.G. (2013), "Semi-analytical solution for electromagnetothermo-elastic creep response of functionally graded piezoelectric rotating disk", *Int. J. Therm. Sci.*, **65**, 254-266.

Loghman, A., Hammami, M. and Loghman, E. (2017), "Effect of the silicon-carbide micro- and nanoparticle size on the thermo-elastic and time-dependent creep response of a rotating Al–SiC composite cylinder", *J. Appl. Mech. Techn. Phys.*, **58**(3), 443-453.

Loghman, A., Faegh, R.K. and Arefi, M. (2018), "Two dimensional time-dependent creep analysis of a thick-walled FG cylinder based on first order shear deformation theory", *Steel Compos. Struct., Int. J.*, **26**(5), 533-547.

Mendelson, A. (1968), *Plasticity Theory and Applications*, The Macmillan Company

Mirsky, I. (1959), *Axially Symmetric Motions of Thick Cylindrical Shells*.

Nguyen, T.-K., Vo, T.P. and Thai, H.-T. (2013), "Static and free vibration of axially loaded functionally graded beams based on the first-order shear deformation theory", *Compos. Part B: Eng.*, **55**, 147-157.

Niknam, H., Fallah, A. and Aghdam, M.M. (2014), "Nonlinear bending of functionally graded tapered beams subjected to thermal and mechanical loading", *Int. J. Non-Linear Mech.*, **65**, 141-147.

Oh, Y. and Yoo, H.H. (2016), "Vibration analysis of rotating pretwisted tapered blades made of functionally graded materials", *Int. J. Mech. Sci.*, **119**, 68-79.

Rao, J.S. and Vyas, N.S. (1996), "Determination of Blade Stresses Under Constant Speed and Transient Conditions With Nonlinear Damping", *J. Eng. Gas Turb. Power*, **118**(2), 424-433.

Sahan, M.F. (2015), "Transient analysis of cross-ply laminated shells using FSDT: Alternative formulation", *Steel Compos. Struct., Int. J.*, **18**(4), 889-907.

Sankar, B.V. (2001), "An elasticity solution for functionally graded beams", *Compos. Sci. Tech.*, **61**(5), 689-696.

Sankar, B.V. and Tzeng, J.T. (2002), "Thermal Stresses in Functionally Graded Beams", *AIAA Journal*, **40**(6), 1228-1232.

Shi, G., Lam, K.Y. and Tay, T.E. (1998), "On efficient finite element modeling of composite beams and plates using higher-

order theories and an accurate composite beam element", *Compos. Struct.*, **41**(2), 159-165.

CC

Appendix A

$$B_1(x) = \int_{-\frac{g(x)}{2}}^{\frac{g(x)}{2}} E(x)dz$$

$$B_2(x) = \int_{-\frac{g(x)}{2}}^{\frac{g(x)}{2}} zE(x)dz$$

$$B_3(x) = \int_{-\frac{g(x)}{2}}^{\frac{g(x)}{2}} G(x)dz$$

$$B_4(x) = \int_{-\frac{g(x)}{2}}^{\frac{g(x)}{2}} z^2E(x)dz$$

$$B_5(x) = \int_{-\frac{g(x)}{2}}^{\frac{g(x)}{2}} E(x)\alpha(x)dz$$

$$B_6(x) = \int_{-\frac{g(x)}{2}}^{\frac{g(x)}{2}} E(x)\alpha(x)zdz$$

Appendix B

$$B_1(x^k) = \int_{-\frac{g(x^k)}{2}}^{\frac{g(x^k)}{2}} E(x^k)dz$$

$$B_2(x^k) = \int_{-\frac{g(x^k)}{2}}^{\frac{g(x^k)}{2}} zE(x^k)dz$$

$$B_3(x^k) = \int_{-\frac{g(x^k)}{2}}^{\frac{g(x^k)}{2}} G(x^k)dz$$

$$B_4(x^k) = \int_{-\frac{g(x^k)}{2}}^{\frac{g(x^k)}{2}} z^2E(x^k)dz$$

$$B_5(x^k) = \int_{-\frac{g(x^k)}{2}}^{\frac{g(x^k)}{2}} E(x^k)\alpha(x^k)T(x)dz$$

$$B_6(x^k) = \int_{-\frac{g(x^k)}{2}}^{\frac{g(x^k)}{2}} E(x^k)\alpha(x^k)T(x)zdz$$